First-principles investigation on ideal strength of B2 NiAl and NiTi alloys*

Chun-Yao Zhang(张春尧), Fu-Yang Tian(田付阳)†, and Xiao-Dong Ni(倪晓东)‡

Institute for Applied Physics, University of Science and Technology Beijing, Beijing 100083, *China*

(Received 7 August 2019; revised manuscript received 30 December 2019; accepted manuscript online 10 February 2020)

For B2 NiAl and NiTi intermetallic compounds, the ideal stress–strain image is lack from the perspective of elastic constants. We use first-principles calculation to investigate the ideal strength and elastic behavior under the tensile and shear loads. The relation between the ideal strength and elastic constants is found. The uniaxial tension of NiAl and NiTi along ⟨001⟩ crystal direction leads to the change from tetragonal path to orthogonal path, which is driven by the vanishing of the shear constant C_{66}. The shear failure under $\{110\}\langle 111\rangle$ shear deformation occurring in process of tension may result in a small ideal tensile strength (~ 2 GPa) for NiTi. The unlikeness in the ideal strength of NiAl and NiTi alloys is discussed based on the charge density difference.

Keywords: ideal strength, stress–strain, elastic constants, first-principles calculation, NiAl and NiTi, charge density difference

PACS: 62.20.de, 64.70.qd, 74.20.Pq **DOI:** 10.1088/1674-1056/ab7440

1. Introduction

The NiAl intermetallic compound has attracted extensive attention as the high-temperature structural material due to its advantages such as high melting point, low density, high thermal conductivity, good oxidation resistance, etc.[1–4] Whereas NiAl exhibits the poor ductility at room temperature. The B2 NiAl alloy is composed of Ni atoms and Al atoms with a simple cubic shifted by 1/2 along the diagonal direction, with the mixed metallic and covalent bonding. Different from NiAl, the B2 NiTi alloy has been widely applied in the industry as the functional material due to its excellent shape memory effect.[5] However, the oxidation resistance at high temperature is not good and its low hardness is also a factor restricting its further extensive application. In theoretical and experimental sides, extensive works focus on the mechanical properties of NiAl and NiTi.[6–11] For instance, the shear deformation of NiAl occurs prior to tensile deformation according to the ideal tensile and shear deformation. The B2 NiAl exhibits strongly intrinsic brittleness.[12] The study of the Fe and Mn metal elements doped NiAl alloy indicated that Fe improves the ductility of NiAl.[13,14] The elastics in NiTi alloy suggested that the shear modulus C_{44} at high temperature is involved in the martensitic transformation.[15]

As one of the most important physical parameters, the elastic constants are often used to evaluate the response of the material to various internal and external stresses.[16,17] When the strain of the material is small, the relationship of stress–strain satisfies the Hooke's law as follows:

$$\begin{pmatrix} \sigma_{xx} \\ \sigma_{yy} \\ \sigma_{zz} \\ \tau_{yz} \\ \tau_{zx} \\ \tau_{xy} \end{pmatrix} = \begin{pmatrix} C_{11} & C_{12} & C_{13} & C_{14} & C_{15} & C_{16} \\ C_{21} & C_{22} & C_{23} & C_{24} & C_{25} & C_{26} \\ C_{31} & C_{32} & C_{33} & C_{34} & C_{35} & C_{36} \\ C_{41} & C_{42} & C_{43} & C_{44} & C_{45} & C_{46} \\ C_{51} & C_{52} & C_{53} & C_{54} & C_{55} & C_{56} \\ C_{61} & C_{62} & C_{63} & C_{64} & C_{65} & C_{66} \end{pmatrix} \begin{pmatrix} \varepsilon_{xx} \\ \varepsilon_{yy} \\ \varepsilon_{zz} \\ \gamma_{yz} \\ \gamma_{zx} \\ \gamma_{xy} \end{pmatrix}, \quad (1)$$

where σ represents the tensile stress, τ for the shear stress, ε for the tensile strain, and γ represents the shear strain. The elastic constants are crucial for a sound understanding of the mechanical properties of the relevant materials. Mouhat[18] *et al.* studied the necessary and sufficient elastic stability conditions in various crystal systems. Although many works on B2 NiAl and NiTi were done, the physical mechanism of stress–strain images generated by the tension and shear deformation is still unclear. The accurate calculation of the ideal strength is necessary for the theoretical study of the inherent mechanical properties of NiAl and NiTi.

First-principles method is a powerful tool to predict the atomic physical properties of materials.[19–23] It has been widely used in the past decades to calculate the elastic modulus, ideal tensile, and shear strength of pure metals and intermetallic compounds.[8,12,15,24–28] The purpose of this paper is to give a physical interpretation of the stress–strain images of NiAl and NiTi from the perspective elastic coefficients by using the first-principles calculation.

*Project supported by the Science Challenge Project, China (Grant No. TZ2018002) and the Fundamental Research Funds for the Central Universities, China (Grant No. FRF-TP-18-013A3).

†Corresponding author. E-mail: fuyang@ustb.edu.cn

‡Corresponding author. E-mail: nixiaodong@ustb.edu.cn

2. Calculated details

In this study, first-principles calculation was carried out by using the Cambridge Sequential Total Energy Package (CASTEP)[29] based on the density functional theory.[30,31] The generalized gradient approximation treated by Perdew–Burke–Ernzerhof[32] was used for the exchange–correlation functionals. The plane-wave cutoff energy was 400 eV for the tensile (shear) deformation configurations. The on-the-fly-generator (OTFG) ultrasoft pseudopotentials were used to represent the interactions between the ionic cores and the valence electrons.[33] For the irreducible Brillouin zone, the Monkhorst–Pack scheme was employed for k points sampling and the density parameter was 0.04 Å^{-1} for the tensile and shear deformation configurations.[34] We chose a high convergence tolerance level (the energy is about 10^{-6} eV/atom, the max force is about 0.01 eV/Å, and the max stress is about 0.02 GPa). The Broyden, Fletcher, Goldforb, Shanno (BFGS)[35] proposed optimized algorithm was used to obtain the equilibrium lattice parameter, the ground-state energy, and the force constants.[36] We extracted the elastic constants from the force constants based on the stress–strain relation, further obtained the polycrystalline elastic moduli by using the arithmetic Hill average of the Voigt and Reuss bounds.[37]

3. Results and discussion

Table 1 lists the calculated equilibrium lattice parameter, three independent elastic constants for the cubic crystal, and derived elastic moduli as well as the available experimental results including bulk modulus B, shear modulus G, and Young's modulus E. Our theoretical lattice parameters (2.893 Å for NiAl and 3.003 Å for NiTi) are in excellent agreement with the experimental results (2.89 Å for NiAl and 3.01 Å for NiTi).[38,39] The present calculated elastic constants of NiAl are in good agreement with the experiments, while for NiTi the calculated elastic constants are slightly larger than the experimental results. Note that the shear constant C' is consistent with the experimental result for NiTi. From Table 1, we can find that the elastically anisotropic parameters $C_{44}/C' > 1$ for NiAl and NiTi are close to each other. It indicates that the Young's modulus along $\langle 111 \rangle$ crystal direction is the largest among all crystal directions of B2 NiAl and NiTi. The calculated elastic moduli B, G, E and Poisson ratio ν are very close to the experimental results. The elastic moduli of NiAl are larger than those of NiTi. According to the following equations:[40]

$$E_{\langle 001 \rangle} = \frac{(C_{11}-C_{12})(C_{11}+2C_{12})}{C_{11}+C_{12}}, \tag{2}$$

$$E_{\langle 110 \rangle} = \left[\frac{(C_{11}+C_{12})}{(C_{11}+2C_{12})(C_{11}-C_{12})} + \frac{1}{4}\left(\frac{1}{C_{44}}-\frac{2}{C_{11}-C_{12}}\right)\right]^{-1}, \tag{3}$$

$$E_{\langle 111 \rangle} = \left[\frac{(C_{11}+C_{12})}{(C_{11}+2C_{12})(C_{11}-C_{12})} + \frac{1}{3}\left(\frac{1}{C_{44}}-\frac{2}{C_{11}-C_{12}}\right)\right]^{-1}, \tag{4}$$

we calculated Young's moduli of NiAl and NiTi along the three typical crystal directions (see Table 1). The Young's moduli of NiAl and NiTi are both arranged in the order of $E_{\langle 111 \rangle} > E_{\langle 110 \rangle} > E_{\langle 001 \rangle}$. It suggests that the tensile deformation along $\langle 001 \rangle$ crystal direction is easy with respect to other crystal directions. NiTi has smaller Young's modulus in the three crystal directions compared to NiAl.

Table 1. The lattice parameter a (in Å), elastic constants C_{11}, C_{12}, C_{44} (in GPa), elastic moduli B, G, E (in GPa), Poisson ratio ν, and Young's moduli along different crystal directions.

	a	C_{11}	C_{12}	C_{44}	C'	C_{44}/C'	B	G	E	$E_{\langle 001 \rangle}$	$E_{\langle 110 \rangle}$	$E_{\langle 111 \rangle}$	ν
NiAl	2.893	208.2	134.5	118.4	36.9	3.2	159.1	74.3	192	102.6	197.2	284.6	0.30
Expt.[12]	2.89	199	137	116	31	3.7	158	76	188	87	180	279	0.31
NiTi	3.003	181.5	152.3	50.2	14.6	3.5	162	30.7	86.6	42.5	87.9	136.5	0.41
Expt.[41]	3.01	162	132	36	15	2.4	159	32	90	43	75	100	0.41

For the energy–strain and stress–strain relationships, a series of incremental strains were applied to the crystal, and the total energy and stress were firstly calculated as a function of the strain. At each step of the strain, the atomic position and structural parameters were fully relaxed while keeping the applied strain fixed. Along the $\langle 001 \rangle$ crystal direction, the uniaxial tension along the body centered tetragonal (bct) path, the cell deformation from bcc to face centered cubic (fcc) is shown in Fig. 1(a). Considering that the orthogonal strain path may occur before the ideal strength up to maximum along the bct path, we define the orthorhombic strain path as the face centered orthogonality (fco) path (shown in Fig. 1(b)). The configurations of tensile deformation along $\langle 110 \rangle$ and $\langle 111 \rangle$ crystal directions are shown in Figs. 1(c) and 1(d). The $\{110\}\langle 111 \rangle$ and $\{211\}\langle 111 \rangle$ shear deformations are shown in Figs. 1(e) and 1(f).

The relationships between the structural parameters, energy vs. strain, and stress vs. strain in the tensile and shear processes are shown in Figs. 2–4. For the tensile along the bct path, we show in Figs. 2(a) and 2(b) the lattice parameters as a function of the tensile strain. The lattice parameters a and b are fully relaxed under the tensile load. Both a and b decrease

with increasing strain, and remain equal with each other. For the fco path, a and b shown in Figs. 2(c) and 2(d) are equal and decrease linearly in the range $\varepsilon = 0$–0.36 for NiAl and $\varepsilon = 0$–0.33 for NiTi, with the increase of the tensile strain. Beyond $\varepsilon = 0.36$ for NiAl and $\varepsilon = 0.33$ for NiTi, a bifurcation occurs because of lattice parameter $a \neq b$.

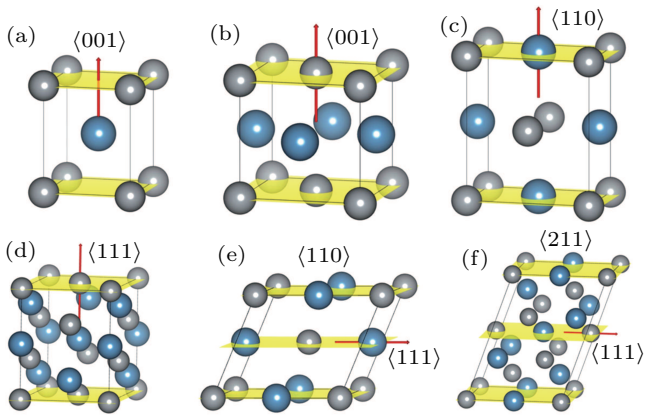

Fig. 1. Configurations of tensile and shear deformations. Panels (a) and (b) are bct and fco paths along ⟨001⟩ crystal direction, (c) and (d) are those along ⟨110⟩ and ⟨111⟩ crystal directions, respectively. (e) and (f) The configurations for $\{110\}\langle 111\rangle$ and $\{211\}\langle 111\rangle$ shear deformations.

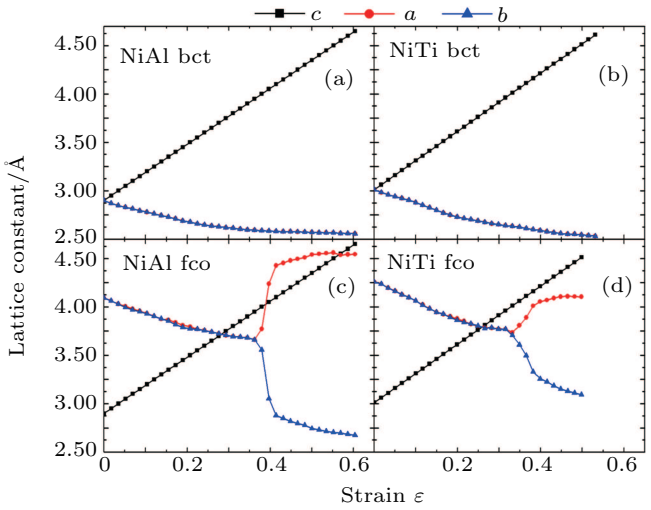

Fig. 2. The lattice parameters a, b, and c as a function of the strain Σ: (a), (b) for bct path and (c), (d) for fco path.

Figure 3 shows the energy difference ΔE as a function of the strain. It can be seen that the energy goes up as the strain increases. For NiAl and NiTi, the initial growth rate of energy along the ⟨111⟩ crystal direction is the largest during the tensile process (see Figs. 3(a) and 3(b)). In the ⟨001⟩ crystal direction, the energy difference ΔE along the bct path is the same as that in the fco path ($\varepsilon = 0$–0.36 for NiAl and $\varepsilon = 0$–0.33 for NiTi). The overall trend of energy vs. strain image of NiAl is very similar to that of NiTi, except that when the strain $\varepsilon = 0$–0.2, the energy of NiTi increases slowly and the energy starts to increase significantly beyond $\varepsilon = 0.2$.

For the shear deformation, we can find from Fig. 3(c) (Fig. 3(d)) that the ΔE under $\{110\}\langle 111\rangle$ ($\{211\}\langle 111\rangle$) shear deformation in NiTi increases linearly as a function of shear strain $\Sigma = 0$–0.28 (0–0.18), whereas the corresponding shear stain $\Sigma = 0$–0.08 occurs in NiAl. It may suggest that NiTi has good elastically deformed behavior and shape memory effect. The energy difference under $\{211\}\langle 111\rangle$ shear deformation is larger compared to that under $\{110\}\langle 111\rangle$.

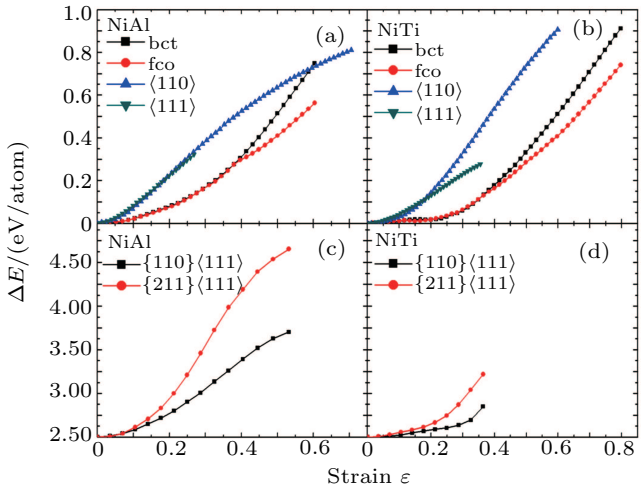

Fig. 3. The energy difference ΔE as a function of strain Σ: (a), (b) for the tensile deformation and (c), (d) for the shear deformation.

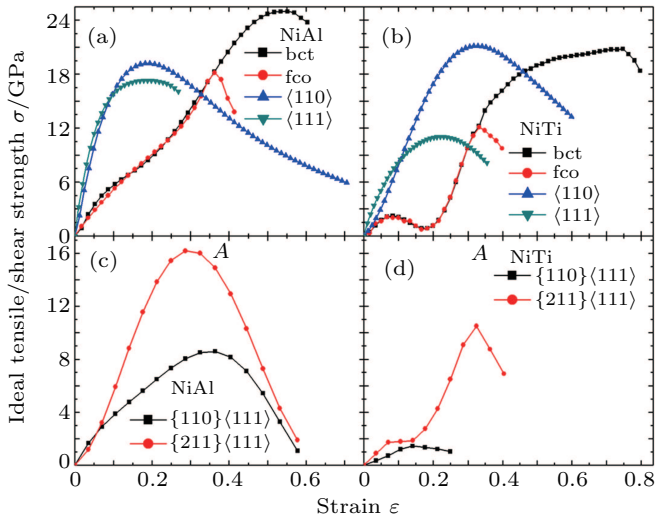

Fig. 4. The ideal strength σ as a function of strain Σ: (a), (b) for the tensile deformation and (c), (d) for the shear deformation.

The variation of the ideal tensile strength is shown in Figs. 4(a) and 4(b). Table 2 summarizes the ideal strength and the corresponding strain under different deformations. The order of the initial slope value of the image is [111] > [110] > [001], which is consistent with the data of Young's modulus listed in Table 1. The overall trend of the stress–strain image under tensile load for NiAl is very similar to that for NiTi, except that there is a small peak along ⟨001⟩ tension for NiTi before the bifurcation ($\varepsilon = 0.33$). The stress–strain image along the bct path is almost the same as that along the fco path before the bifurcation ($\varepsilon = 0.36$ for NiAl, $\varepsilon = 0.33$ for NiTi) occurs. The lowest ideal tensile strength of NiAl is along the ⟨111⟩

crystal direction, which is different from the lowest strength of NiTi along the ⟨001⟩ crystal direction. The ideal shear strength is shown in Figs. 4(c) and 4(d). The ideal strength under {211}⟨111⟩ shear is much greater than that under {110}⟨111⟩, indicating an anisotropic characteristics along the ⟨111⟩ crystal direction.

Table 2. Ideal tensile and shear strain ε and strength σ of NiAl and NiTi.

	Deformation	ε	σ
NiAl	⟨001⟩ bct	0.55	24.9
	⟨001⟩ fco	0.36	18.1
	⟨110⟩	0.19	19.2
	⟨111⟩	0.19	17.3
	{110}⟨111⟩	0.36	8.6
	{211}⟨111⟩	0.29	16.2
NiTi	⟨001⟩ bct	0.08	2.2
	⟨001⟩ fco	0.08	2
	⟨110⟩	0.33	21.1
	⟨111⟩	0.22	11
	{110}⟨111⟩	0.14	1.4
	{211}⟨111⟩	0.32	10.5

In order to better understand the tensile and shear behaviors, we study the elastic constants under tensile and shear loads. There are 21 independent constants in the generalized elastic tensor which relates stress and strain in an anisotropic medium. The number of independent elastic constants depends on the lattice symmetry. For NiAl and NiTi, we calculated the elastic coefficients during tension along the bct (the tetragonal lattice is observed) path. Due to the lattice parameter $a = b \neq c$ and the basic vector's orthogonality in the tetragonal crystal system, we can derive the following equations from Eq. (1):

$$\begin{aligned}
\sigma_{xx} &= C_{11}\varepsilon_{xx} + C_{12}\varepsilon_{yy} + C_{13}\varepsilon_{zz},\\
\sigma_{yy} &= C_{12}\varepsilon_{xx} + C_{11}\varepsilon_{yy} + C_{13}\varepsilon_{zz},\\
\sigma_{zz} &= C_{13}\varepsilon_{xx} + C_{13}\varepsilon_{yy} + C_{33}\varepsilon_{zz},\\
\tau_{yz} &= C_{44}\gamma_{yz},\\
\tau_{zx} &= C_{44}\gamma_{zx},\\
\tau_{xy} &= C_{66}\gamma_{xy}.
\end{aligned} \tag{5}$$

There are only 6 independent elastic constants in Eq. (5) for the tetragonal lattice. σ_{xx} (ε_{xx}), σ_{yy} (ε_{yy}), and σ_{zz} (ε_{zz}) represent the tensile stress (strain) along the x-axis, y-axis, and z-axis. τ_{yz} (γ_{yz}), τ_{zx} (γ_{zx}), and τ_{xy} (γ_{xy}) represent the shear stress (strain) along the y–z plane, z–x plane, and x–y plane, respectively. Figure 5 shows the variation of the elastic coefficients for NiAl and NiTi under uniaxial strain along the bct path. From the strain of $\varepsilon = 0.34$ for NiAl and $\varepsilon = 0.35$ for NiTi, we can find the elastic constant $C_{66} \leq 0$ from Fig. 6, which results in the x–y plane shear failure according to Eq. (5). Because of the x–y plane shear failure, we can observe that both $a \neq b$ and bifurcation occur when the tension is along the fco path. Our calculations at the deformation ($\varepsilon = 0.34$ for NiAl and $\varepsilon = 0.35$ for NiTi) are in good agreement with the tensile strains shown in Figs. 2(c) and 2(d) ($\varepsilon = 0.36$ for NiAl and $\varepsilon = 0.33$ for NiTi). From Eq. (5), we can see that C_{13} and C_{33} are the first partial derivative of σ_{zz} with respect to ε. Figure 6 shows $C_{13} < 0$ and $C_{33} \leq 0$ at the strain $\varepsilon = 0.58$ for NiAl and $\varepsilon = 0.76$ for NiTi, which indicates that the slope of the stress–strain image of the bct path should be negative or zero. The results are consistent with the conclusion shown Figs. 4(a) and 4(b). $C_{11} > |C_{12}|$ is the necessary and sufficient conditions for the elastic stability in tetragonal classes,[18] violating this condition occurs at the strain of $\varepsilon = 0.08$–0.17 for NiTi in Fig. 5. This may be the reason why there is a small wave peak along ⟨001⟩ tension ($\varepsilon = 0.08$–0.18) of NiTi. By analyzing the NiTi structure when it is stretched along the path of ⟨001⟩ to reach the ideal strength, we speculate that it might be caused by the shear failure under {110} ⟨111⟩ during the stretching process.

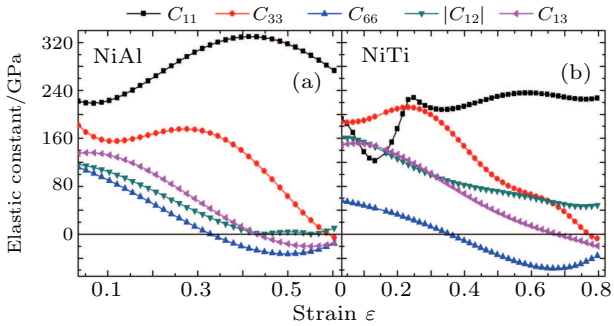

Fig. 5. The elastic coefficients as a function of tensile strain Σ along the bct path: (a) for NiAl and (b) for NiTi.

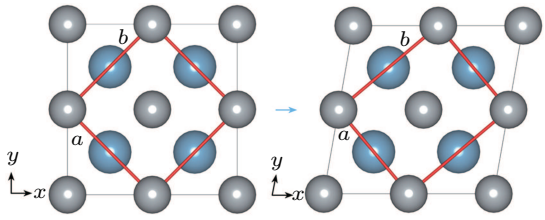

Fig. 6. The shear failure occurs on plane x–y due to $C_{66} < 0$.

Figure 7 shows the charge density difference in the {110} plane family under tensile and shear loads. We can see that the charge density near Ni atoms is larger than that near Al and Ti. It suggests that the charge transfers from Al and Ti to Ni, i.e., Ni atoms obtain charge from Al and Ni. The charge density locates on the Al and Ni atoms in NiAl, while the charge density is slightly delocalized in NiTi. It may indicate that the metallic bonding exits in NiAl alloys. With the increase of the tensile and shear loads, the image of charge difference near Ti and Ni extremely changes, while the image of charge difference keeps unchanged in NiAl. The bonding direction between Ni and Ti extremely changes, which may indicate that the bonding is relatively weak between Ni and Ti, then the tensile and shear deformation occurs easily in NiTi.

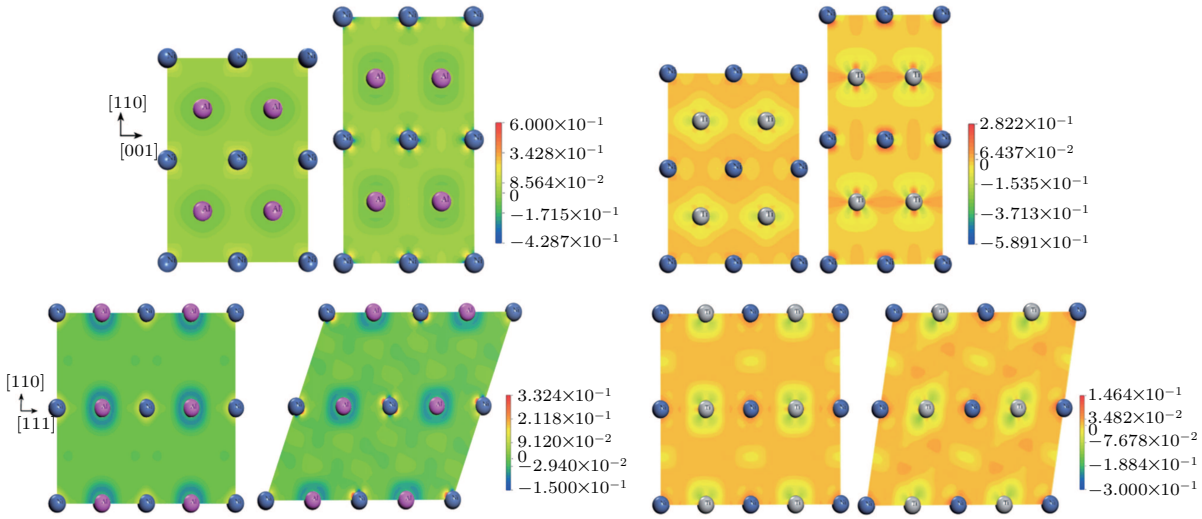

Fig. 7. The charge density difference under tensile and shear loads for NiAl and NiTi.

4. Conclusion

First-principles calculation based on density functional theory was applied to study the ideal strength and elastic constants during the tensile and shear strain processes for the B2 NiAl and NiTi alloys. Our conclusions are drawn as follows.

(i) For the body centered tetragonal and faced orthogonal paths, the lattice parameters of NiAl and NiTi as a function of strain are very close to each other. However, the ideal tensile strength and shear strength of NiAl are 18.1 GPa at $\Sigma = 0.36$ along the faced orthogonal path and 8.6 GPa at $\Sigma = 0.36$ under $\{110\}\langle 111\rangle$ shear, respectively. Whereas the corresponding results in NiTi are only $\sigma = 2$ GPa at $\Sigma = 0.36$ along the faced orthogonal path and $\sigma = 1.4$ GPa at $\Sigma = 0.14$ under $\{110\}\langle 111\rangle$ shear.

(ii) For the ideal tension along $\langle 001\rangle$ crystal direction, the vanishing of the elastic constant C_{66} causes the x–y plane shear failure. It causes the transformation from the tetragonal path to the orthogonal path. The maximum ideal tensile strength along the tetragonal path is determined by C_{13} and C_{33}. The reason why the ideal tensile strength of NiTi along $\langle 001\rangle$ crystal direction is smaller than that of NiAl may be that the shear failure under $\{110\}\langle 111\rangle$ shear deformation occurs during the tensile process.

(iii) The image of charge difference in the $\{110\}$ plane family further suggests that the tensile and shear deformations of NiTi easily occur, compared to NiAl.

References

[1] Raynolds J E, Smith J R, Zhao G L and Srolovitz D J 1996 *Phys. Rev. B* **53** 13883
[2] Zhang X Y, Sprengel W, Reichle K J, Blaurock K, Henes R and Schaefer H E 2003 *Phys. Rev. B* **68** 224102
[3] Korzhavyi P A, Ruban A V, Lozovoi A Y, Vekilov Y K, Abrikosov I A and Johansson B 2000 *Phys. Rev. B* **61** 6003
[4] Lui S C, Davenport J W, Plummer E W, Zehner D M and Fernando G W 1990 *Phys. Rev. B* **42** 1582
[5] Casalena L, Bigelow G S, Gao Y, Benafan O, Noebe R D, Wang Y and Mills M J 2017 *Intermetallics* **86** 33
[6] Hansen K H, Gottschalck J, Petersen L, Hammer B, Laegsgaard E, Besenbacher F and Stensgaard I 2001 *Phys. Rev. B* **63** 115421
[7] Mishin Y, Mehl M J and Papaconstantopoulos D A 2002 *Phys. Rev. B* **65** 224114
[8] Hatcher N, Kontsevoi O Y and Freeman A J 2009 *Phys. Rev. B* **80** 144203
[9] Zarkevich N A and Johnson D D 2014 *Phys. Rev. B* **90** 060102
[10] Chen Z, Qin S, Shang J, Wang F and Chen Y 2018 *Intermetallics* **94** 47
[11] Mahmud A, Wu Z, Zhang J, Liu Y and Yang H 2018 *Intermetallics* **103** 52
[12] Xing H, Dong A, Huang J, Zhang J and Sun B 2018 *J. Mater. Sci. & Technol.* **34** 620
[13] Lazar P and Podloucky R 2009 *Intermetallics* **17** 675
[14] Lazar P and Podloucky R 2006 *Phys. Rev. B* **73** 104114
[15] Lu J M, Hu Q M and Yang R 2009 *J. Mater. Sci. & Technol.* **25** 215
[16] Tanaka K and Koiwa M 1996 *Intermetallics* **4** S29
[17] Jamal M, Jalali Asadabadi S, Ahmad I and Rahnamaye Aliabad H A 2014 *Comput. Mater. Sci.* **95** 592
[18] Mouhat F and Coudert F X 2014 *Phys. Rev. B* **90** 224104
[19] Zhang N N, Zhang Y J, Yang Y, Zhang P and Ge C C 2019 *Chin. Phys. B* **28** 046301
[20] He X and Li J B 2019 *Chin. Phys. B* **28** 037301
[21] Wu J H and Liu C X 2016 *Chin. Phys. Lett.* **33** 036202
[22] Lei B, Zhang Y Y and Du S X 2019 *Chin. Phys. B* **28** 046803
[23] Wang F N, Li J C, Li Y, Zhang X M, Wang X J, Chen Y F, Liu J, Wang C L, Zhao M L and Mei L M 2019 *Chin. Phys. B* **28** 047101
[24] Jhi S H, Louie S G, Cohen M L and Morris J W Jr 2001 *Phys. Rev. Lett.* **87** 075503
[25] Nagasako N, Asahi R and Hafner J 2012 *Phys. Rev. B* **85** 024122
[26] Li T, Morris J W, Jr., Nagasako N, Kuramoto S and Chrzan D C 2007 *Phys. Rev. Lett.* **98** 105503
[27] Nagasako N, Jahnátek M, Asahi R and Hafner J 2010 *Phys. Rev. B* **81** 094108
[28] Qi L and Chrzan D C 2014 *Phys. Rev. Lett.* **112** 115503
[29] Segall M D, Lindan P J D, Probert M J, Pickard C J, Hasnip P J, Clark S J and Payne M C 2002 *J. Phys-Condens Mat* **14** 2717
[30] Kohn W and Sham L J 1965 *Phys. Rev.* **140** A1133
[31] Hohenberg P and Kohn W 1964 *Phys. Rev. B* **136** B864
[32] Perdew J P, Burke K and Ernzerhof M 1996 *Phys. Rev. Lett.* **77** 3865
[33] Vanderbilt D 1990 *Phys. Rev. B* **41** 7892
[34] Wisesa P, McGill K A and Mueller T 2016 *Phys. Rev. B* **93** 155109
[35] Güler M and Güler E 2013 *Chin. Phys. Lett.* **30** 056201
[36] Chen Z, Fei P and Zhou Y 1995 *Acta Math. Sci.* **15** 283
[37] Hill R 1952 *Proc. Phys. Soc. A* **65** 349
[38] Davenport T, Zhou L and Trivisonno J 1999 *Phys. Rev. B* **59** 3421
[39] Hosoda H and Inamura T 2009 *Shape Memory Alloys for Biomedical Applications* (New York: CRC Press) pp. 20–36
[40] Li X, Schönecker S, Li W, Varga L K, Irving D L and Vitos L 2018 *Phys. Rev. B* **97** 094102
[41] Sanati M, Albers R C and Pinski F J 1998 *Phys. Rev. B* **58** 13590